International Journal of Solids and Structures 56–57 (2015) 43–52

Contents lists available at ScienceDirect

International Journal of Solids and Structures

journal homepage: www.elsevier.com/locate/ijsolstr

Predicting hygro-elastic properties of paper sheets based on an idealized model of the underlying fibrous network

Emanuela Bosco [a,b,*], Ron H.J. Peerlings [b], Marc G.D. Geers [b]

[a] Materials innovation institute (M2i), P.O. Box 5008, 2600 GA Delft, The Netherlands
[b] Department of Mechanical Engineering, Eindhoven University of Technology, P.O. Box 513, 5600 MB Eindhoven, The Netherlands

ARTICLE INFO

Article history:
Received 25 March 2014
Received in revised form 20 October 2014
Available online 15 December 2014

Keywords:
Fibrous material
Meso-structural model
Hygro-expansive deformation

ABSTRACT

Significant dimensional variations may occur in paper-based materials when subjected to changes in moisture content. Moisture induced deformations are governed by the swelling of individual fibres, which is transferred through inter-fibre bonds to the entire fibrous network. Complex interactions between mechanical and hygro-expansive properties take place in the bonding areas, affecting the overall material response. In most network models, the role of these inter-fibre bonds is not explicitly incorporated. This work presents a periodic meso-structural model for the discrete fibrous network, which considers the free-standing fibre segments *and* inter-fibre bonds. Despite its simplicity, the reference unit-cell enables the incorporation of relevant micro- and meso-structural features such as network structure, fibres and bond geometry and hygro-elastic properties. The proposed model is solved analytically through a proper homogenization strategy, allowing to recover the paper's anisotropic hygro-mechanical response in terms of effective elastic constants and effective hygro-expansive coefficients, exploiting the coupling at the meso-structural level between hygroscopic and mechanical behavior. A comparison with experimental results obtained from the literature shows that the presented approach is quite accurate in predicting the overall paper response, thereby revealing the influence of several meso-scale parameters (e.g. fibre orientation, dimensions, mechanical strength).

1. Introduction

Paper is a material consisting of cellulose fibres bonded to each other to form a discrete network (Niskanen, 1998). Due to the production process, fibres have a preferential orientation along the direction of manufacturing, resulting in a significant anisotropy of the material. A distinctive feature of paper is its sensitivity to changes in moisture content, which lead to pronounced dimensional variations at different length scales. The hygro-expansive response of paper originates at the fibre level, where a single fibre exhibits strongly anisotropic moisture induced deformations. The fibres' hygro-expansive behavior is transferred within the meso-structural network through the inter-fibre bonds, where micro-stresses generally appear due to the interaction between mechanical and hygro-expansive properties of the fibres (Larsson and Wagberg, 2008). All of these phenomena in the underlying fibrous structure concur to yield the overall moisture induced deformations at the sheet level, which can be represented with reasonable approximation through a linear relation with respect to the humidity variation (Nanri and Uesaka, 1993). Hygro-expansive strains significantly influence the industrial performance of the material, for instance in relation to the runnability during printing operations. Understanding how the effective properties of paper are controlled by the hygro-mechanical response of individual fibres and the fibrous network is thus highly relevant for industrial and engineering applications.

Discrete meso-structural models are particularly appropriate to understand how the deformation mechanisms at the micro-structural level determine the macroscopic continuum response, as they allow to directly incorporate single paper fibres as individual constituents of the discrete fibrous network. In the literature, several publications deal with mechanical descriptions of paper based on stochastic analytical or computational network models (Cox, 1952; Ostoja-Starzewski, 1998; Stahl and Cramer, 1998; Bronkhorst, 2003; Ramasubramanian and Wang, 2007; Strömbro and Gudmundson, 2008; Strömbro and Gudmundson, 2008; Liu et al., 2010; Liu et al., 2011; Kulachenko and Uesaka, 2012). These approaches describe an individual paper fibre as a chain of trusses (e.g. in Cox (1952)) or beams (e.g. in Bronkhorst, 2003;

* Corresponding author at: Department of Mechanical Engineering, Eindhoven University of Technology, P.O. Box 513, 5600 MB Eindhoven, The Netherlands. Tel.: +31 40 247 5169.
E-mail address: e.bosco@tue.nl (E. Bosco).

http://dx.doi.org/10.1016/j.ijsolstr.2014.12.006
0020-7683/

Ostoja-Starzewski and Stahl, 2000) that are connected to each other through inter-fibre bonds, which are generally identified with the nodes. Commonly, fibres are modeled with an axial stiffness only; in Schulgasser and Page (1988), the transverse properties are included as well. The existing network models are generally reliable in quantifying mechanical properties at the sheet level, either in the elastic (Ostoja-Starzewski and Stahl, 2000) or in the visco-elastic (Strömbro and Gudmundson, 2008; Strömbro and Gudmundson, 2008) or in the elasto-plastic (Bronkhorst, 2003; Ramasubramanian and Wang, 2007; Liu et al., 2011) range.

Effective hygro-expansive properties of paper can be obtained through a classical homogenization approach (Rosen and Hashin, 1970; Hashin, 1983), which provides hygro-expansive coefficients for a general anisotropic composite as a function of the hygro-elastic properties of the phases with an arbitrary geometry. Specifying the expression for a fibrous network is, however, not trivial. In Uesaka (1994), the hygro-expansive behavior of paper is interpreted through the analysis of the phenomena occurring at the mesoscopic scale. Both mechanical and hygro-expansive properties (in the longitudinal and transverse direction) of a single fibre contribute to the effective response of the material. In particular, the degree of macroscopic stress transferred within the network throughout the inter-fibre bonds governs the effective hygro-expansivity. An important role of hygro-mechanical interactions within fibre bonding zones is thus suggested. This approach can explain in a qualitative way a number of experimental results (Uesaka, 1994; Uesaka and Qi, 1994); however, a strategy to compute the hygro-expansive coefficients explicitly is not at hand. Also more generally, to the best of our knowledge, the literature lacks of models which are dedicated, based on the analysis of fibre level and network characteristics, to predict the resulting hygro-expansive behavior of paper.

In this contribution, a novel meso-structural model of paper is elaborated that bridges the hygro-mechanical properties at the fibre level to the effective response of the material. The fibrous network is simplified to a two dimensional periodic lattice structure, using a unit-cell with elements in four directions. The effect of the fibre orientation distribution, which is responsible for the paper's anisotropic behavior, is included in the geometrical characterization of the unit-cell. Free-standing fibre segments are considered as trusses. In the literature, a pin-jointed bond model is frequently adopted, see e.g. Bronkhorst (2003). However, this bond description is unrealistic, as the size of the bond (i.e. approximatively the fibre width) is of the same order as the inter-fibre spacing. Moreover, at the origin of the resulting hygro-expansive behavior of paper lies the coupling between the hygroscopic and mechanical properties of fibres in the bonding zones, which cannot be captured through pin-jointed bonds.

A distinctive aspect of this work is the fact that the inter-fibre bonds are modeled explicitly, and they are treated as laminated composite plates. The bonds incorporate both the longitudinal and transverse hygro-mechanical properties of the intersecting fibres, and thus contribute to the effective material response. Internal stresses in the bonds due to hygro-mechanical loads can be naturally represented. Elastic constitutive behavior has been considered for both fibre segments and bonds, restricting the present analysis to the macroscopic hygro-elastic behavior. However, in principle, different constitutive choices can be made for the meso-structural components in order to capture inelastic deformations and stress relaxation at the sheet level. The proposed lattice model is idealized, but for that reason extremely powerful. First, it can be solved analytically. Moreover, while allowing to extract the effective material properties in a simple manner, it offers additional insight in the elementary mechanisms connecting fibres up to the resulting behavior at the sheet level. All relevant features of the mesoscopic structure are explicitly taken into account: the geometry of fibres and bonds; the network structure through the fibre orientation distribution; and the anisotropic mechanical and hygroscopic properties of single fibres via their constitutive behaviors. Note finally that, even if the exact small scale constitutive and geometric parameters are not fully experimentally identified, the proposed model may help to understand qualitatively how sheet scale properties depend on network properties, and hence how to improve or tailor the macroscopic response by manipulating the network features.

This paper is organized as follows. In Section 2, the proposed meso-structural unit-cell model is defined together with the underlying assumptions on the network geometry and the fibre/bond constitutive behavior. The homogenization procedure used to extract the effective material properties is also detailed. An illustrative example is presented in Section 3, where the elastic and hygro-expansive properties calculated with the presented methodology are compared with experimental data extracted from the literature. Concluding remarks are given in Section 4.

Throughout the paper, the following notations for Cartesian tensors and tensor products are used: $a, \mathbf{a}, \mathbf{A}$, and ${}^{n}\mathbf{A}$ denote, respectively, a scalar, a vector, a second-order tensor, and an nth-order tensor. The following notation for vector and tensor operations is employed together with Einstein's summation convention: the dyadic product $\mathbf{a} \otimes \mathbf{b} = a_i b_j \mathbf{e}_i \otimes \mathbf{e}_j$, and the inner products $\mathbf{A} \cdot \mathbf{b} = A_{ij} b_j \mathbf{e}_i, \mathbf{A} \cdot \mathbf{B} = A_{ij} B_{jk} \mathbf{e}_i \otimes \mathbf{e}_k, \mathbf{A} : \mathbf{B} = A_{ij} B_{ji}$, with $\mathbf{e}_i$ ($i = x, y, z$ for the global reference system and $i = \ell, t, z$ for the local reference system) the unit vectors of a Cartesian vector basis. Voigt notation is used to represent tensors and tensor operations in a matrix form: a column and a matrix of scalars are indicated as a and $\underline{A}$, respectively. The matrix multiplication is defined as $(\underset{\sim}{\underline{A}\, b})_i = A_{ij} b_j$, together with Einstein's summation convention.

2. Hygro-mechanical model

2.1. Target macroscopic model

The interactions at the meso-structural level between physical and geometrical properties of fibres play a fundamental role in determining the resulting material properties of paper. In order to assess the overall paper behavior, a macroscopic description must incorporate a detailed characterization of the fibres' mechanical response, dimensions, nature of inter-fibre bonds and the geometry of the network. From a macroscopic perspective, when a sheet of paper is exposed to a uniform change in the moisture content χ, the stress free hygro-expansive strain can be quantified as

$$\boldsymbol{\varepsilon}_h = \boldsymbol{\beta}\chi \tag{1}$$

where $\boldsymbol{\beta}$ is the tensor of effective hygro-expansive coefficients. If no external loads are applied, the average stress is zero, but internal stresses may arise in the fibre network. In addition, if macroscopic mechanical stresses are considered, in an elastic network, the total strain $\boldsymbol{\varepsilon}$ can be expressed as the sum of an elastic and a hygro-expansive part

$$\boldsymbol{\varepsilon} = \boldsymbol{\varepsilon}_e + \boldsymbol{\varepsilon}_h \tag{2}$$

and the following constitutive relation can be written

$$\boldsymbol{\sigma} = {}^{4}\mathbf{C} : (\boldsymbol{\varepsilon} - \boldsymbol{\beta}\chi) \tag{3}$$

where ${}^{4}\mathbf{C}$ is the effective elastic stiffness tensor of the paper. The objective of this contribution is to predict $\boldsymbol{\beta}$ as well as ${}^{4}\mathbf{C}$, given the properties of the fibrous network.

2.2. Proposed meso-structural model

The global reference system (x, y, z) is taken to be aligned with the principal directions of paper, i.e. the machine direction (MD), the cross direction (CD) and the thickness direction. Fibre segments are mainly oriented within the (x, y) plane so paper can be approximated as a two dimensional system subjected to in-plane loads. The present analysis is therefore based on a two dimensional plane stress model: the deformations in the z direction will be taken into consideration a posteriori for the evaluation of the out-of-plane hygro-expansive coefficient.

The meso-structural network of paper fibres is idealized trough a lattice model with a rectangular unit-cell which contains fibres oriented at the angles $0, \pi/2$ and $\pm\bar{\theta}$ with respect to the x-axis. Although in principle different choices of $\bar{\theta}$ can be made, the following derivations will be specified for $\bar{\theta} = \pi/4$, reducing the model to a square unit-cell, whose geometry is shown in Fig. 1(a). A single fibre is characterized by a rectangular cross section of thickness h and width w. Bonds are identified at the intersection between four fibres. The edge of the square bonding area is w. The length l of a unit-cell edge, i.e. the idealized distance between the barycentres of two fibre bonds, can be expressed as $l = l^f + w$, where l^f denotes the free-standing fibre segment's length in MD and CD.

To describe the probability density function of the fibre orientation in the network structure of paper, a wrapped Cauchy orientation distribution curve is often used in the literature, see e.g. Cox (1952):

$$f(\theta) = \frac{1}{\pi}\frac{1-q^2}{1+q^2-2q\cos(2\theta)} \tag{4}$$

where $-\pi/2 < \theta \leqslant \pi/2$ is the angle between a fibre and the machine direction, and $0 \leqslant q < 1$. Fig. 1(b) (top) shows the profile of the orientation distribution function for different values of the parameter q. For $q = 0$, the curve reduces to a uniform distribution, i.e. the isotropic case. As q increases, the fibres are most prominently aligned along the machine direction. The proposed model naturally includes the effect of fibre orientation by integrating at four discrete angles, $\boldsymbol{\theta} = [0; \pi/2; \pm\pi/4]$, the orientation probability density function (4) and by obtaining the corresponding weight factors $\lambda^{(k)}$ with $\sum_{k=1}^{4}\lambda^{(k)} = 1$, as shown in Fig. 1(b) (bottom). Note that for the symmetry of (4), $\lambda^{(3)} = \lambda^{(4)}$. The weights $\lambda^{(k)}$ are then used to define a corrected thickness for the fibres oriented at each of the four angles $\theta^{(k)}$, i.e. $h^{(k)} = \lambda^{(k)}h$.

Bonds are treated as laminated composite plates, in which each layer (k) is represented by the volume of a single fibre participating in the bonding area. The total thickness of the bond is thus given by $h = \sum_k h^{(k)}$, see Fig. 1(a) representing the bond cross section. Note that in the further derivations, only the ratio between the thicknesses of the fibres and the thickness of the bond matters; therefore only the weights $\lambda^{(k)}$, and not the value of h, will constitute a parameter for the model. The connection between fibres and bonds is described through frictionless hinges: the forces acting in the free-standing fibre segments are transmitted through the hinges to the bond, and, in an equilibrium state, they must be in balance with the average bond stress.

For the illustrated geometry of the model and a given fibre width, the length l of a unit-cell edge can be calculated from the mass equality between the continuum level and the network level:

$$l \approx w\frac{\lambda^{(1)} + \lambda^{(2)} + \lambda^{(3)}/\cos\bar{\theta} + \lambda^{(4)}/\cos\bar{\theta}}{c} \tag{5}$$

where $c = \rho/\rho_f$ is the mean areal coverage of the paper, defined as the ratio between paper density $\rho$and fibre wall density ρ_f. For a given value of paper coverage, l depends on the coefficient q of the fibre orientation distribution (4) through the ratios $\lambda^{(k)}$.

The key-assumptions adopted for the proposed model are next detailed. Free-standing fibre segments can swell freely as moisture content varies, while in the bonding regions they constrain each other giving rise to hygro-mechanical interactions. The entire unit cell experiences the same moisture content variation χ. At the same time, the network may also be loaded mechanically. These

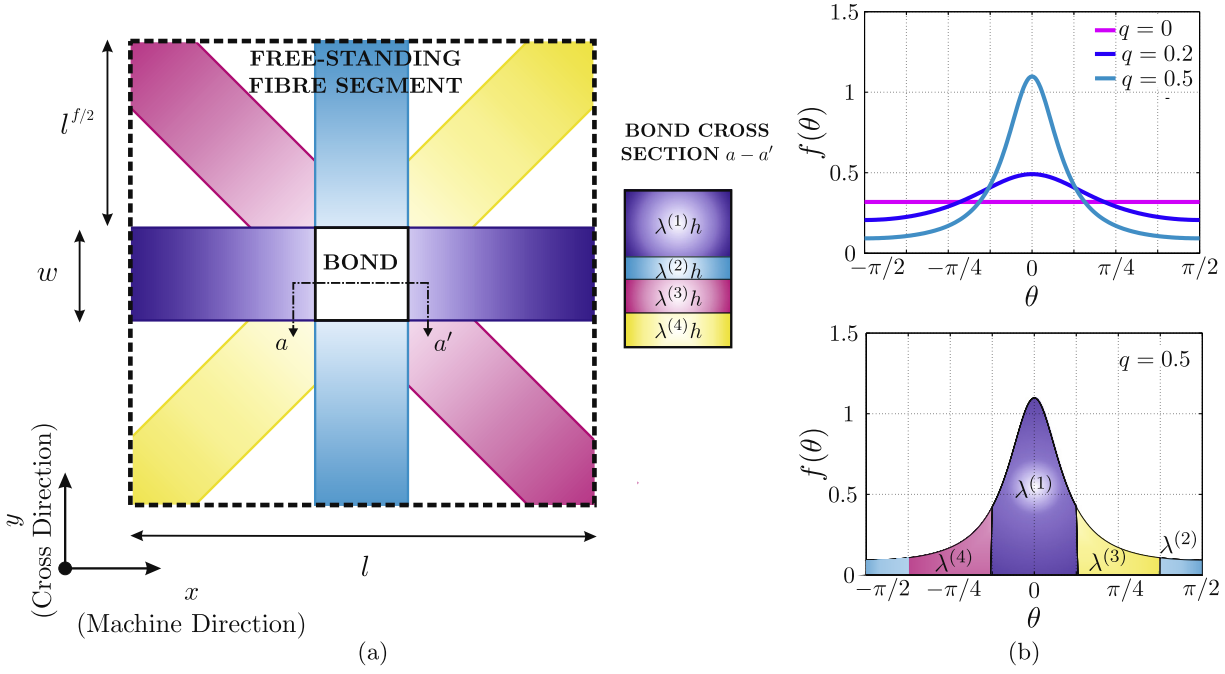

Fig. 1. (a) Geometry of the unit-cell used to extract the effective material properties of paper. (b) Fibre orientation distribution function shown for different values of the parameter q (top). Weight ratios $\lambda^{(k)}$ for each of the four angles $\theta^{(k)}$, illustrated with different colours, for the case $q = 0.5$ (bottom).

two loading conditions determine the overall response of the material, expressed by the effective hygro-mechanical properties $\boldsymbol{\beta}$ and ${}^4\mathbf{C}$.

2.3. Fibre constitutive model

Consider a local coordinate system (ℓ, t, z) taken along the principal directions of a fibre. Paper fibres are commonly assumed to be transversely isotropic in their hygro-mechanical properties with respect to their longitudinal axis ℓ (Bergander and Salmèn, 2002). Assuming a plane stress state in z-direction, the general constitutive law for a fibre reads

$$\boldsymbol{\sigma}^f = {}^4\mathbf{C}^f : \left(\boldsymbol{\varepsilon}^f - \boldsymbol{\beta}^f \chi\right) \tag{6}$$

where ${}^4\mathbf{C}^f$ and $\boldsymbol{\beta}^f$ are the transversely isotropic elasticity tensor and the fibre's hygro-expansivity tensor, respectively. In Voigt notation, their corresponding matrix format reads

$$\underset{\sim}{C}^f = \begin{pmatrix} \frac{E_\ell}{(1-\nu_{\ell t}\nu_{t\ell})} & \frac{\nu_{t\ell}E_\ell}{(1-\nu_{\ell t}\nu_{t\ell})} & 0 \\ \frac{\nu_{\ell t}E_t}{(1-\nu_{\ell t}\nu_{t\ell})} & \frac{E_t}{(1-\nu_{\ell t}\nu_{t\ell})} & 0 \\ 0 & 0 & G_{\ell t} \end{pmatrix}; \quad \underset{\sim}{\beta}^f = \begin{pmatrix} \beta_\ell \\ \beta_t \\ 0 \end{pmatrix} \tag{7}$$

The constants E_ℓ and E_t are the moduli of elasticity along and transverse to the fibre axis, respectively; $G_{\ell t}$ is the in-plane shear modulus and $\nu_{\ell t}$ and $\nu_{t\ell}$ the in-plane Poisson's ratios, with $E_\ell \nu_{t\ell} = E_t \nu_{\ell t}$. The parameters β_ℓ and β_t characterize the longitudinal and transverse hygro-expansive coefficients of the fibre, respectively. For further reference, the elastic strain component in the z direction can be written in terms of the in-plane strains as

$$\varepsilon^f_{zz,e} = \frac{\nu_{\ell t}(1+\nu_{zt})}{1-\nu_{\ell t}\nu_{t\ell}}\varepsilon^f_{\ell\ell,e} + \frac{\nu_{\ell t}\nu_{t\ell}+\nu_{zt}}{1-\nu_{\ell t}\nu_{t\ell}}\varepsilon^f_{tt,e} \tag{8}$$

Note finally that, although the elastic constants of fibres may generally vary as a function of the moisture content, they will be assumed to be moisture independent.

Each free-standing fibre segment is considered to be stress-free in the lateral direction, i.e. behaving as a linear elastic truss with stiffness E_ℓ and hygro-expansive coefficient β_ℓ. Hooke's law holds as specified in (6), which in this one dimensional representation simplifies to

$$\sigma^f = E_\ell(\varepsilon^f - \beta_\ell \chi) \tag{9}$$

where the subscript $\ell\ell$ has been omitted for the sake of simplicity. The transverse deformation due to both elastic and hygro-expansive strains is ignored in the free-standing fibre segments. Note that also the shear deformation is neglected; the effective shear response will be defined by the contribution of the diagonal elements of the unit-cell. This is also commonly done in the literature, see e.g. (Bronkhorst, 2003; Strömbro and Gudmundson, 2008; Kulachenko and Uesaka, 2012).

2.4. Bond constitutive model

In the bonded area, the hygro-elastic transverse deformation cannot be neglected. The interplay between the longitudinal and transverse stiffnesses and hygro-expansive coefficients constrains the hygro-expansion and induces micro-stresses, influencing the effective properties of the material. This important coupling effect is incorporated in the model through the definition of a proper behavior for the bond. The shear deformation is also taken into account here as it contributes in defining the effective bond response.

To recover the bond equivalent properties, the constitutive quantities (7) referring to the local reference system (ℓ, t) of a fibre oriented at angle $\theta^{(k)}$ have to be expressed with respect to the global reference system (x, y) – see e.g. Roylance (1996):

$$\underline{C}^{(k)} = \left[\underline{R}(\underline{A}^{(k)})^{-1}\underline{R}^{-1}(\underline{C}^f)^{-1}\underline{A}^{(k)}\right]^{-1} \tag{10}$$

$$\underset{\sim}{\beta}^{(k)} = \underline{R}\underline{A}^{(k)}\underline{R}^{-1}\underset{\sim}{\beta}^f \tag{11}$$

where $\underline{A}^{(k)}$ and $\underline{R}$ are the transformation matrix and the Reuters matrix, defined as

$$\underline{A}^{(k)} = \begin{pmatrix} c^2 & s^2 & 2sc \\ s^2 & c^2 & -2sc \\ -sc & sc & c^2-s^2 \end{pmatrix}, \quad \underline{R} = \begin{pmatrix} 1 & 0 & 0 \\ 0 & 1 & 0 \\ 0 & 0 & 2 \end{pmatrix} \tag{12}$$

with $c = \cos\theta^{(k)}, s = \sin\theta^{(k)}$.

In view of the hygro-expansive deformations, the bond constitutive behavior can be written as

$$\boldsymbol{\sigma}^b = {}^4\mathbf{C}^b : (\boldsymbol{\varepsilon}^b - \boldsymbol{\beta}^b \chi) \tag{13}$$

where ${}^4\mathbf{C}^b$ and $\boldsymbol{\beta}^b$ are the bond effective stiffness and effective hygro-expansivity tensors. To obtain these overall properties, a Voigt average is used, i.e. full kinematic compatibility is assumed between the fibre layers composing the bond. For the kth fibre, the compatibility condition reads

$$\boldsymbol{\varepsilon}^b = \boldsymbol{\varepsilon}^{f(k)} \tag{14}$$

while the stress in the bond is obtained as the volume average

$$\boldsymbol{\sigma}^b = \sum_{k=1}^{4} \lambda^{(k)} \boldsymbol{\sigma}^{f(k)} \tag{15}$$

where $\boldsymbol{\sigma}^{f(k)}$ is given by Eq. (6), specified for the corresponding $\theta^{(k)}$ with the tensor form of (10) and (11). Substituting (13) and (6) into (15) and considering (14), the following expressions for the bond's effective hygro-elastic constants are derived,

$${}^4\mathbf{C}^b = \sum_{k=1}^{4} \lambda^{(k)} {}^4\mathbf{C}^{(k)} \tag{16}$$

$$\boldsymbol{\beta}^b = \left({}^4\mathbf{C}^b\right)^{-1} : \sum_{k=1}^{4} \left(\lambda^{(k)} {}^4\mathbf{C}^{(k)} : \boldsymbol{\beta}^{(k)}\right) \tag{17}$$

which have to be inserted in Eq. (13).

An additional consideration can be made on how the bonded fibres interact within the bond area and, at the same time, the bond interacts with the external, free-standing fibre segments. Eq. (15) defines the average stress in the bond. Global force equilibrium applies between the bond and the connected free-standing fibres. Assuming that both the bonds and the free-standing fibre segments are in a uniform stress state, the stress in the bond can be interpreted as a surface average of the sum of the axial forces in the converging free-standing fibre segments:

$$\boldsymbol{\sigma}^b = \frac{1}{A^b}\sum_{k=1}^{4} F^{f(k)} \mathbf{n}^{(k)} \otimes \mathbf{n}^{(k)} \tag{18}$$

where $A^b = wh$ is the lateral area of the bond in contact with the crossing fibres. The unit vector associated to the axis of the kth free-standing fibre segment oriented at $\theta^{(k)}$ is given as $\mathbf{n}^{(k)} = \cos\theta^{(k)}\mathbf{e}_x + \sin\theta^{(k)}\mathbf{e}_y$; $F^{f(k)} = A^{(k)}\sigma^{f(k)}$ denotes the axial force in the corresponding fibre of cross section $A^{(k)} = h^{(k)}w = \lambda^{(k)}hw$. The symmetry of the stress $\boldsymbol{\sigma}^b$ is preserved as $\mathbf{n}^{(k)} \otimes \mathbf{n}^{(k)}$ is by definition symmetric. For a schematic one-dimensional interpretation of Eqs. (15) and (18), refer to Fig. 2.

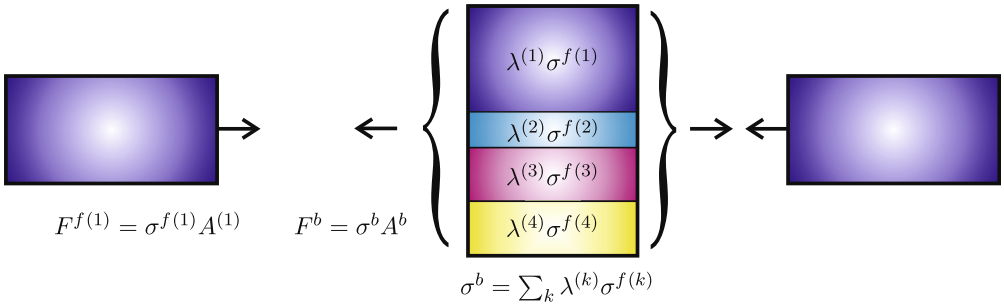

Fig. 2. One dimensional interpretation of the fibres interaction within the bonded area and the bond interaction with the connected free-standing fibre segments.

2.5. Effective material properties

The effective hygro-mechanical material properties of the paper are extracted analytically from the unit-cell through a proper homogenization procedure. To determine the effective elastic constants, consider an external in-plane mechanical load at a constant moisture content which produces a uniform stress state $\boldsymbol{\sigma}$ in the homogeneous effective material. From equilibrium, this stress state has to be in balance with the stress in the unit-cell

$$\boldsymbol{\sigma}A = \boldsymbol{\sigma}^b A^b = \sum_{k=1}^{4} F^{f(k)}\mathbf{n}^{(k)} \otimes \mathbf{n}^{(k)} \tag{19}$$

where $A = lh$ is the lateral area of a unit-cell edge; the last equality follows from (18). Between the strain $\boldsymbol{\varepsilon}$, associated to $\boldsymbol{\sigma}$, the strain in the free-standing fibre segments $\varepsilon^{f(k)}$ and the strain in the bonds $\boldsymbol{\varepsilon}^b$, a Reuss-like averaging relation can be written:

$$l^{(k)}\mathbf{n}^{(k)} \cdot \boldsymbol{\varepsilon} \cdot \mathbf{n}^{(k)} = l^{f(k)}\varepsilon^{f(k)} + w\mathbf{n}^{(k)} \cdot \boldsymbol{\varepsilon}^b \cdot \mathbf{n}^{(k)}, \quad k = 1,2,3,4 \tag{20}$$

with $l^{(k)} = l, l^{f(k)} = l^f$ for $k = 1,2; l^{(k)} = l/\cos\theta^{(k)}, l^{f(k)} = l^f/\cos\theta^{(k)}$ for $k = 3,4$. Note that expression (20) for the strain average together with (18) satisfy the energy consistency between the internal work in the bond and the work exerted on the bond by the connecting fibres.

The system of equations consisting of equilibrium (19), strain compatibility (20) and constitutive behavior (3), (9) and (13) can be solved for different external loads, to obtain the effective property of interest. For instance, in order to identify the effective elastic modulus E_{xx} and the Poisson's ratio ν_{xy}, one needs to consider a uni-axial stress state in the $x$direction at a constant moisture content. The only non-zero component in the left hand side of equilibrium (19) is σ_{xx}. Moreover, from constitutive relation (3) follows that $\sigma_{xx} = E_{xx}\varepsilon_{xx}$ and $\varepsilon_{yy} = -\nu_{xy}\varepsilon_{xx}$. Constitutive expressions (9), (13) and (3), specialized as above, are substituted in (19), allowing to write the system in terms of the strain components. From this immediately follows that the shear deformation in the bond vanishes and that, through the symmetry of the problem, the diagonal fibres are subjected to an equal strain. The remaining components $\varepsilon^b_{xx}, \varepsilon^b_{yy}$ of the bond strain and the strains $\varepsilon^{f(k)}$ in the free-standing fibre segments can be expressed as a function of the macroscopic deformation ε_{xx}. Substituting the obtained strain expressions in Eq. (20), leads to the effective elastic modulus E_{xx} and the Poisson's ratio ν_{xy}.

Following the same reasoning for a uni-axial load in the y direction and for a shear load, allows one to obtain the effective elastic modulus E_{yy} and the Poisson's ratio ν_{yx}, and the shear modulus G_{xy}, respectively. The values of the effective elastic properties are written as

$$E_{xx} = \frac{c_1 E_\ell \left(C^b_{xx}C^b_{yy} - C^{b^2}_{xy}\right)}{c_2\left(C^b_{xx}C^b_{yy} - C^{b^2}_{xy}\right) + E_\ell\left(c_3 C^b_{yy} + c_4 C^b_{xy}\right)} \tag{21}$$

$$E_{yy} = \frac{c_1 E_\ell \left(C^b_{xx}C^b_{yy} - C^{b^2}_{xy}\right)}{c_5\left(C^b_{xx}C^b_{yy} - C^{b^2}_{xy}\right) + E_\ell\left(c_6 C^b_{xx} + c_7 C^b_{xy}\right)} \tag{22}$$

$$G_{xy} = \frac{c_{13} E_\ell G^b_{xy}}{c_{14} G^b_{xy} + c_{15} E_\ell} \tag{23}$$

$$\nu_{xy} = \frac{c_8\left(C^b_{xx}C^b_{yy} - C^{b^2}_{xy}\right) + c_9 C_{yy} E_\ell + c_{10} C_{xy} E_\ell}{c_2\left(C^b_{xx}C^b_{yy} - C^{b^2}_{xy}\right) + E_\ell\left(c_3 C^b_{yy} + c_4 C^b_{xy}\right)} \tag{24}$$

$$\nu_{yx} = \frac{c_8\left(C^b_{xx}C^b_{yy} - C^{b^2}_{xy}\right) + c_{11} C_{xx} E_\ell + c_{12} C_{xy} E_\ell}{c_5\left(C^b_{xx}C^b_{yy} - C^{b^2}_{xy}\right) + E_\ell\left(c_6 C^b_{xx} + c_7 C^b_{xy}\right)} \tag{25}$$

where the full expressions for the coefficients c_m, with $m = 1, \ldots, 15$, are given in Appendix A. The obtained elastic constants are dependent on the fibre's mechanical properties and geometry and on the network structure. It can be verified that the Maxwell relation holds, i.e. $E_{xx}\nu_{yx} = E_{yy}\nu_{xy}$.

An analogous procedure can be used to calculate the in-plane effective hygro-expansive coefficients β_{xx} and β_{yy}. Note that, according to the choice of the global reference system along the material's principal directions, $\beta_{xy} = 0$. Considering a uniform variation of the moisture content with homogeneous boundary conditions, i.e. $\boldsymbol{\sigma} = \mathbf{0}$, the total deformation is expressed by (1). The fibre segments are allowed to freely deform with $\sigma^{f(k)} = 0$; moreover, from equilibrium (19) it follows that $\boldsymbol{\sigma}^b = \mathbf{0}$. Note that although the total stress in the bond is zero, internal stresses arise in the layers of the bond due to the misorientation between the different fibres passing through the bond. The strains in the bond $\boldsymbol{\varepsilon}^b$ and in the free-standing fibres $\varepsilon^{f(k)}$ are thus given only by their hygro-expansive contribution. Condition (20) thus reduces to

$$\beta_{xx} = \frac{1}{l}\left(l^f \beta_\ell + w\beta^b_{xx}\right) \tag{26}$$

$$\beta_{yy} = \frac{1}{l}\left(l^f \beta_\ell + w\beta^b_{yy}\right) \tag{27}$$

A final consideration can be made on the effective out-of-plane hygro-expansive coefficient β_{zz}. As the transverse hygro-expansive deformation of the free-standing fibre parts may be accommodated by the free space around them, β_{zz} is governed only by the bond response and it can be calculated as the out of plane hygro-expansive coefficient of the bond itself, by using relation (17) together with (16). The single fibre constitutive tensor, hygro-expansive coefficients (7) and the transformation matrices (12) should then be written considering also the components related to direction z. Taking into account that the fibres are assumed to be transversely isotropic, the additional material parameters of interest are $E_z = E_t, \nu_{\ell z} = \nu_{\ell t}, \nu_{tz} = \nu_{zt}$ and $\beta_z = \beta_t$. The fibres are free

to expand in the z direction. Note that due to the plane-stress state assumption, the out-of plane shear components to deformation vanish and thus do not play any role in the derivation of the coefficient β_{zz}, and neither does the more complicated geometry that the bond may have in reality. The value of β_{zz} obtained from (17) can be then interpreted as the sum of the contributions of the transverse hygro-expansive coefficient β_t and of the elastic strain $\varepsilon^f_{zz,e}$ (8) due to the Poisson's effect, for each of the single fibre layers.

3. Results and discussion

In this section, the hygro-elastic behavior of the idealized network model is illustrated and compared to experimental data obtained from the literature.

3.1. Fibre and network parameters used

The macroscopic parameters chosen for the analysis have been extracted from several publications. Softwood fibres are considered, whose geometry is defined by their thickness $w = 35$ μm (Niskanen, 1998). The average length l of the unit-cell edge is calculated according to (5). Its value ranges between 130 and 298 μm as a function of the degree of fibre orientation along machine direction and of the paper and fibre densities. For fully collapsed lumen, the fibre wall density can be approximated as $\rho_f = 1500$ kg/m^3 (Niskanen, 1998). Two different kinds of paper are considered: high density paper with $\rho^{(1)} = 420$ kg/m^3 and low density paper with $\rho^{(2)} = 220$ kg/m^3. Under the hypothesis of moisture independent elastic constants, the longitudinal elastic stiffness is taken as $E_\ell = 44$ GPa (Strömbro and Gudmundson, 2008). The elastic modulus in the transverse direction and the shear modulus can be defined as functions of the longitudinal stiffness through the constants $\alpha = E_\ell/E_t = 6$ and $\gamma = E_\ell/G_{\ell t} = 10$, such that $E_t = 7.3$ GPa, $G_{\ell t} = 4.4$ GPa (Schulgasser and Page, 1988; Bergander and Salmèn, 2002). For these values of the parameters α and γ, the Poisson's ratio of the fibre is taken as $\nu_{\ell t} = 0.3$, (Schulgasser and Page, 1988), $\nu_{t\ell}$ follows from the equality $\nu_{t\ell} = \nu_{\ell t}/\alpha = 0.05$. Experimental data for the fibre shear modulus $G_{\ell t}$ and the Poisson's ratio $\nu_{\ell t}$ are extremely rare in the literature; however, it can be shown that within the proposed approach the values of $G_{\ell t}, \nu_{\ell t}$ influence the resulting in-plane effective properties only mildly. For this reason, the adopted values may be assumed as reasonable input parameters. As no data seems to be available for ν_{zt}, results will be discussed for the cases $\nu_{zt} = 0, \nu_{zt} = \nu_{t\ell}$ and $\nu_{zt} = \nu_{\ell t}$. The hygro-expansive coefficient along the fibre direction is taken as $\beta_\ell = 0.03$, while in the transverse direction the coefficient $\beta_t = 20\beta_\ell = 0.6$ is used (Niskanen, 1998).

3.2. Effective hygro-mechanical properties

The elastic constants of the paper obtained from Eqs. (21) and (22) are shown in Fig. 3(a) as a function of the parameter q, which characterizes the fibre orientation in machine direction. The elastic moduli in machine direction E_{xx} and in cross direction E_{yy} are illustrated for high density (solid magenta lines, $\rho^{(1)}$) and low density (dashed blue lines, $\rho^{(2)}$) paper. As the fibre orientation along the machine direction increases, the stiffness E_{xx} obviously increases while E_{yy} decreases. Both the effective moduli increase with paper density. Typical values for in-plane elastic properties of paper range from 1 to 10 GPa (Niskanen, 2011). The resulting estimates are thus reasonable, especially in the interval $0 \leqslant q \leqslant 0.6$, which corresponds to realistic values for the parameter q. In particular, for $0 \leqslant q \leqslant 0.6$, the ratio between the machine direction and cross direction moduli E_{xx}/E_{yy} varies between 1 and 6, which are common values for paper. In Fig. 3(b), the effective shear modulus G_{xy} calculated through expression (23) is illustrated with solid magenta lines and with dashed blue lines for high and low density paper, respectively. The estimate of G_{xy} decreases with fibre alignment along machine direction. According to Baum et al. (1981), a first approximation for the shear modulus of paper can be given as $G^*_{xy} \approx 1/3(\sqrt{E_{xx}E_{yy}})$. The values of G^*_{xy} are shown in Fig. 3(b) with dash-dot red (high density paper) and cyan lines (low density paper); it can be noticed that they show a reasonable match with the values resulting from (23), especially in the range $0 \leqslant q \leqslant 0.4$.

The effective hygro-expansive constants β_{xx}, β_{yy} of the paper are illustrated in Fig. 4(a) with respect to the degree of fibre alignment along the machine direction. Solid magenta lines represent the coefficients for high density ($\rho^{(1)}$) paper, dashed blue lines denote the coefficients for low density ($\rho^{(2)}$) paper. For increasing values of q, the effective hygro-expansivity coefficients, derived from relations (26), (27), increase in cross direction, while they decrease in machine direction. In machine direction, the hygro-expansivity of the paper is only slightly higher than the longitudinal hygro-expansivity of the fibres $\beta_\ell = 0.03$, which constitutes a lower bond for the estimate. In cross direction the hygro-expansive coefficients are more influenced by the network geometry and by the fibres' mechanical properties and they are thus significantly lower that the upper bound $\beta_t = 0.6$. In particular, for increasing q, β_{yy} approaches the value $(w\beta_t + l^f\beta_\ell)/l < \beta_t$. The effective bond hygro-expansivity β^b_{yy} is in fact predominantly governed by the transverse hygro-expansivity of the fibre oriented along the x-direction and thus converges to β_t, while a fibre oriented along the cross direction still contributes with its longitudinal hygro-expansive deformation, controlled by the coefficient β_ℓ. This is also consistent with the general formula for paper hygro-expansivity presented in Uesaka (1994). Note that the in-plane hygro-expansive coefficients increase with paper density, because the ratio between the bond length and free-standing fibre length is higher and the transverse hygro-expansivity β_t thus contributes in a more significant way. The effect is more evident along the cross direction.

The coefficients β_{zz} have been calculated according to (17) for the three assumed values of ν_{zt}. They are shown in Fig. 4(b) with a dash-dot black line for $\nu_{zt} = \nu_{\ell t}$, a black solid line for $\nu_{zt} = \nu_{t\ell}$ and a black dotted line for $\nu_{zt} = 0; \beta_{xx}, \beta_{yy}$ are replotted in the diagram as a reference. As already mentioned, β_{zz} is not a function of the paper density as it depends only on the behavior of the bond. The out-of-plane hygro-expansive coefficient is significantly higher than the in-plane ones, and it is close to the value of the transverse hygro-expansivity β_t of a single fibre. This is consistent with the physical consideration that paper has a highly oriented structure in the plane (x, y) as observed in Uesaka (1994) and Viguiè et al. (2011). In particular, as fibres are oriented more along machine direction, β_{zz} converges to β_t. Note that the selected values of the fibre Poisson's ratio clearly affect the absolute value of β_{zz}. In the case $\nu_{zt} = \nu_{\ell t}$, the overall elastic deformation due to Poisson's effect occurs in the same direction as the hygro-expansive deformation, while for $\nu_{zt} = 0$ they are opposite in sign. In the case $\nu_{zt} = \nu_{t\ell}$, the elastic strain occurring in the different layers is zero on average, and the resulting hygro-expansive coefficient coincides with the transverse hygro-expansion of the single fibres.

The in-plane hygro-expansive coefficients of Fig. 4(a) can be plotted as a function of the ratio E_{xx}/E_{yy} of the effective moduli in machine direction and cross direction. This enables to compare them with the experimental data presented in Uesaka (1994). The coefficients β_{xx} and β_{yy} are represented in Fig. 5 through solid magenta lines and dashed blue lines for $\rho^{(1)}$ and $\rho^{(2)}$, respectively. The corresponding experimental values are illustrated through magenta squared dots and circular blue dots. The results obtained with the proposed model show a good agreement with the experimental data, especially in machine direction and in cross direction

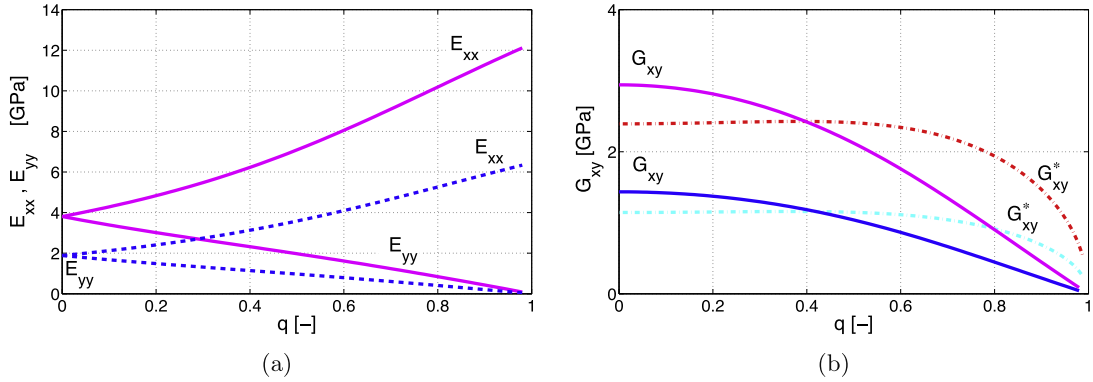

Fig. 3. (a) Effective elastic constants E_{xx}, E_{yy} of paper as a function of the fibre orientation in machine direction. Solid magenta lines denote high density paper ($\rho^{(1)}$) and dashed blue lines refer to low density paper ($\rho^{(2)}$). (b) Comparison between the values of G_{xy} obtained with the proposed model- solid magenta lines for $\rho^{(1)}$ and dashed blue lines for $\rho^{(2)}$) and with the estimate G^*_{xy} of Baum et al. (1981), shown in red ($\rho^{(1)}$) and cyan ($\rho^{(2)}$) dash-dotted lines. (For interpretation of the references to colour in this figure legend, the reader is referred to the web version of this article.)

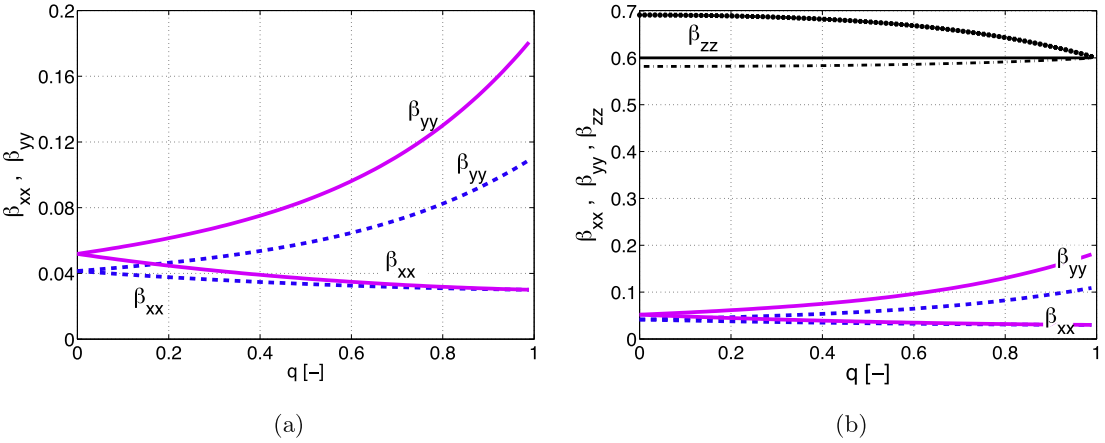

Fig. 4. (a) In-plane effective hygro-expansive coefficients of paper as function of the fibre orientation in machine direction. Solid magenta lines and dashed blue lines represent the coefficients for high ($\rho^{(1)}$) and low ($\rho^{(2)}$) density paper, respectively. (b) Extension of subfigure (a) with the out-of-plane hygro-expansive coefficient β_{zz}, shown with the black dash-dot, solid and dotted line depending on the assumptions made for ν_{zt}. (For interpretation of the references to color in this figure legend, the reader is referred to the web version of this article.)

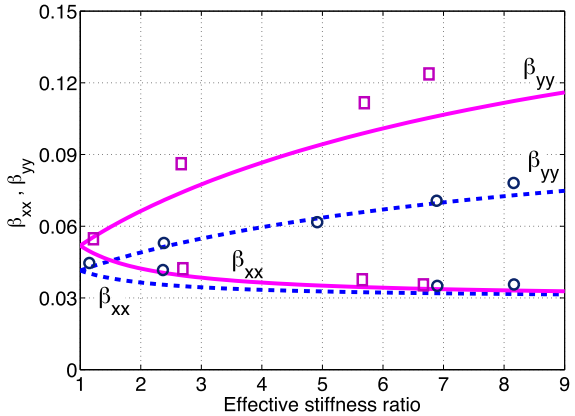

Fig. 5. Comparison between the obtained coefficients β_{xx} and β_{yy} as functions of the effective stiffness ratio and the experimental data presented in Uesaka (1994). Solid magenta and dashed blue curves indicate low and high density paper. The experimental values are illustrated through magenta squared dots and circular blue dots. (For interpretation of the references to colour in this figure legend, the reader is referred to the web version of this article.)

for the low density material. The general formulas for the hygro-expansive coefficients presented in Uesaka (1994) offer a good description of the experimental results. The model proposed in the present paper provides a step forward. Rather than only fitting the experiments, the effective hygro-expansive coefficients can be predicted beforehand, based on the knowledge of the micro- and meso-scale properties, such as hygro-mechanical properties of fibres, fibre geometry and network structure. Results shown here are made without any optimization of the meso-scale parameters to obtain a better match between the macro-prediction and experiments. Nevertheless, despite the high degree of idealization of the network's geometry and large uncertainty in the input parameters at the fibre level, the overall material behavior is well captured.

3.3. Influence of paper density

In Section 3.2, the effective elastic and hygro-expansive properties have been shown for two values of paper density, $\rho^{(1)}$ and $\rho^{(2)}$. The direct influence of the paper density on the effective material response can also be investigated. The effective mechanical and hygro-expansive properties are shown as a function of the paper density ρ normalized with respect to the fibre density ρ_f in Fig. 6(a) and in Fig. 6(b), respectively. The values are referred to two cases: the green dashed lines denote the isotropic case, i.e. $q = 0$; the red solid lines indicate the situation in which $q = 0.5$. As for mechanical properties, both the elastic moduli increase as a function of the normalized paper density; in particular, the cross direction modulus grows with a larger rate for high density paper.

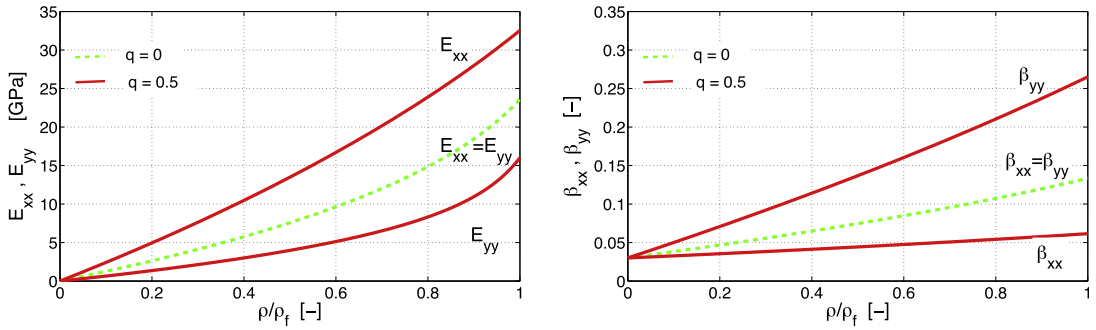

Fig. 6. (a) Effective elastic constants E_{xx}, E_{yy} of paper as a function of the paper density ρnormalized with respect to the fibre density ρ_f. (b) Effective hygro-expansive coefficients β_{xx}, β_{yy} shown with respect to the paper density ratio ρ/ρ_f. In both the diagrams, dashed green lines denote the case $q = 0$, while solid red lines refer to $q = 0.5$. (For interpretation of the references to colour in this figure legend, the reader is referred to the web version of this article.)

The effective hygro-expansive coefficients show an almost linear increase with respect to the normalized paper density, and are more pronouncedly influenced in the cross direction, rather than in the machine direction.

3.4. Internal stresses in the bonds

It may be relevant to calculate the internal stresses induced in the inter-fibre bonds by the hygro-expansive strains. At a given moisture content χ and for an overall stress-free situation, the total deformation of the bond is given as $\boldsymbol{\varepsilon}^b = \boldsymbol{\beta}^b \chi$. In each fibre layer k constituting the bond, the elastic deformation is given by the difference between the total deformation and the fibre hygro-expansive contribution $\boldsymbol{\varepsilon}_h^{(k)} = \boldsymbol{\beta}^{(k)} \chi$. The single fibre internal stress thus reads

$$\boldsymbol{\sigma}^{(k)} = {}^4\mathbf{C}^{(k)} : \left(\boldsymbol{\beta}^b - \boldsymbol{\beta}^{(k)}\right)\chi \tag{28}$$

The obtained values of the internal stresses are illustrated as a function of the moisture content, for a variation of χ up to 0.01. Fig. 7 shows the components $\sigma_{xx}^{(k)}$ (left) and $\sigma_{yy}^{(k)}$ (right). Shear stresses are zero due to the symmetry of the problem. The blue colour refers to the fibre oriented in machine direction, at an angle $\theta^{(1)} = 0$, the cyan colour refers to fibres oriented in cross direction $\theta^{(2)} = \pi/2$, whereas the magenta curves refer to fibres oriented at angles $\theta^{(3),(4)} = \pm\pi/4$. The internal stresses are shown for $q = 0$ (dashed lines) and $q = 0.5$ (continuous lines). The internal stresses have higher absolute values in the cross direction. Even for a limited moisture content variation, relevant stresses arise since stress relaxation is not included in the model. For the isotropic fibre distribution, i.e. $q = 0$, obviously $\sigma_{xx}^{(k)} = \sigma_{yy}^{(k)}$. As a consequence of the Voigt average condition $\sum_k \lambda^{(k)} \boldsymbol{\sigma}^{(k)} = \boldsymbol{\sigma}^b = \mathbf{0}$ holds.

3.5. Influence of number of fibre orientations considered

The hygro-expansive behavior can also be studied using an even simpler unit-cell geometry, which is based on the discretization of the fibre orientation distribution function (4) at two angles only, $\theta^{(1)} = 0$ and $\theta^{(2)} = \pi/2$, i.e. along the machine and the cross direction. This leads to a unit-cell without diagonal elements. The effective hygro-expansive coefficients are again obtained from (26), (27), where the components of $\boldsymbol{\beta}^b$ are calculated considering only two fibre layers. The comparison with the results obtained for the case of four families of fibres is shown in Fig. 8 for low density paper. On the blue dashed curve (already shown in Fig. 4(a)), the cyan solid curved for two families of fibres is superposed. The difference between the two calculations is negligible and governed by the values of the different bond hygro-expansivities. In principle, for an adequate estimate of the hygro-expansivity, the simple two-fibre geometry would be sufficient. However, in terms of mechanical response, a model with diagonal elements is needed, as they provide shear resistance to the unit-cell.

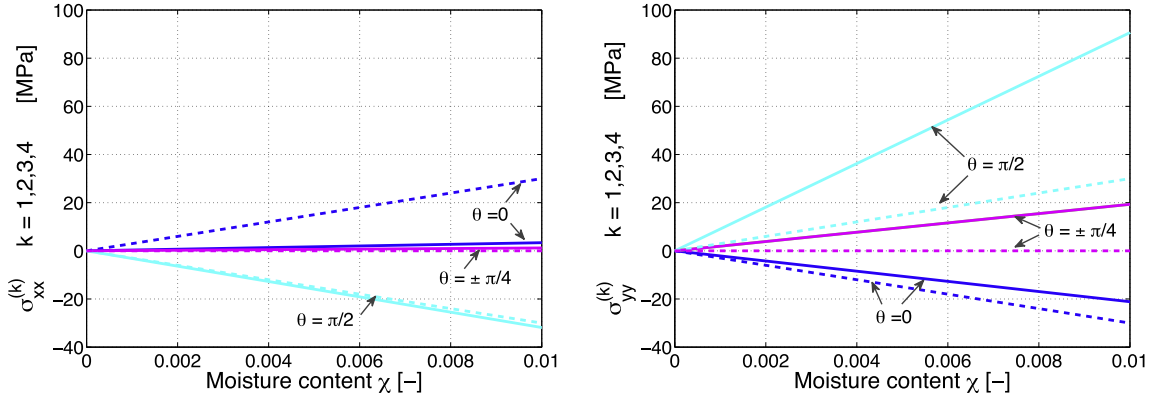

Fig. 7. (a) Internal stresses $\sigma_{xx}^{(k)}$ in the bond layers. (b) Internal stresses $\sigma_{yy}^{(k)}$ in the bond layers. In both figures color blue refers to the fibre oriented at $\theta^{(1)} = 0$, color cyan refers to fibres oriented at $\theta^{(2)} = \pi/2$, magenta curves refer to fibres oriented at angles $\theta^{(3),(4)} = \pm\pi/4$. Dashed lines and solid lines indicate the internal stresses for $q = 0$ and for $q = 0.5$, respectively. (For interpretation of the references to colour in this figure legend, the reader is referred to the web version of this article.)

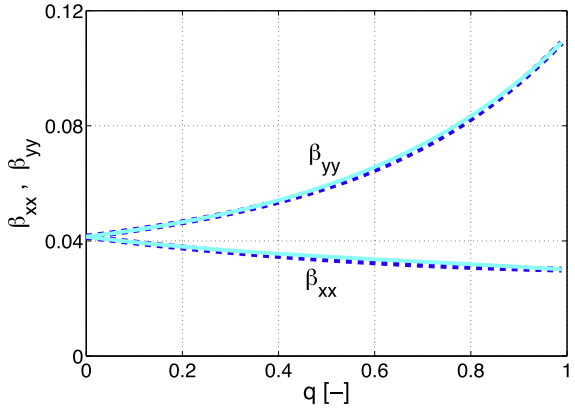

Fig. 8. In-plane effective hygro-expansive coefficients of paper as a function of the fibre orientation in machine direction for low density paper. Solid cyan and dashed blue curves reflect the results for two and four families of fibres, respectively. (For interpretation of the references to color in this figure legend, the reader is referred to the web version of this article.)

4. Conclusions and remarks

This contribution is focussed on the study of the effective hygro-elastic behavior of paper based on the analysis of the underlying fibrous meso-structure.

A two dimensional unit-cell has been used to describe the discrete structure of the network, allowing to incorporate the single fibre's physical and geometrical properties. The anisotropic nature of the network has been included through the fibre orientation distribution function. While free-standing fibre segments have been considered as trusses provided with only axial stiffness and longitudinal hygro-expansive properties, a key aspect of the proposed approach is the description of the inter-fibre bonds through layered composite plates which take into account the transverse properties of the fibres as well. This enables one to naturally analyze the interplay between mechanical and hygro-expansive effects occurring in the bonding area and to study its influence in determining the overall material response. The homogenized results, in terms of effective elastic moduli and hygro-expansivity coefficients extracted from the unit-cell, have been compared with available data from the literature, showing that the relevant characteristics of paper are correctly captured.

The present contribution would certainly benefit from more and more accurate experimental data on both fibre and sheet level properties related to the same paper pulp. This would be useful not only for the purpose of validation of the results, but also for achieving a better insight in the understanding of the material characteristics at the fibre and network scale. For a particular paper of interest, one may obtain a dedicated fibre orientation distribution, and study the actual dimensions of fibres and bonds in relation to their hygro-elastic properties.

A comparison of the proposed unit-cell model with a numerical simulation of a two dimensional or three dimensional network could also contribute in offering more confidence on the obtained results; this aspect will thus be dealt with in a forthcoming publication.

The elastic constants at the fibre level have been taken here to be moisture independent, however their dependency on the moisture content can be incorporated in the model in a straightforward manner.

The work can be further extended to investigate some typical irreversible events which so far have been neglected. During the production process, paper is subjected to tension in machine direction. The induced internal stresses are released when the material is moistened the first time at a sufficient level of moisture. The release of dried-in strains is manifested through an irreversible shrinkage of paper when it returns to the original moisture content. This phenomenon can be explained from a micro-structural point of view through damage accumulation within the free-standing fibres or visco-elastic relaxation of the fibre and/or by the gradual opening of bonds during wetting. The latter could be included in the proposed model by relaxing the full kinematical compatibility assumed for the bond layers by enabling frictional sliding, for instance along the lines of Wilbrink et al. (2013).

The proposed discrete meso-structural model can be finally combined with a computational solution strategy at the sheet level, allowing for the solution of the boundary value problem at the macro-scale with complex hygro-mechanical load cases. This may be done following e.g. Beex et al. (2011).

Acknowledgements

This research was carried out under Project Number M61.2.12458 in the framework of the Research Program of the Materials innovation institute M2i (www.m2i.nl). The authors would like to thank Professor S. Östlund for useful discussions on the topic.

Appendix A. Coefficients of the effective elastic constants

The full expressions of the coefficients which define the elastic constants (21)–(25) are given as:

$$c_1 = A^{(3)}\left(A^{(1)}+A^{(2)}\right)l^f l+\sqrt{2}A^{(1)}A^{(2)}l^{f(3)}l \tag{A.1}$$

$$c_2 = Al^f\left(A^{(3)}l^f+l^{f(3)}A^{(2)}\Big/\sqrt{2}\right) \tag{A.2}$$

$$c_3 = Aw\left(A^{(2)}A^{(3)}l^f\Big/\sqrt{2}+A^{(1)}A^{(3)}l^f+\sqrt{2}A^{(1)}A^{(2)}l^{f(3)}\right)\Big/A^b \tag{A.3}$$

$$c_4 = AA^{(3)}A^{(2)}w\left(1-1/\sqrt{2}\right)l^f\Big/A^b \tag{A.4}$$

$$c_5 = Al^f\left(A^{(3)}l^f+l^{f(3)}A^{(1)}\Big/\sqrt{2}\right) \tag{A.5}$$

$$c_6 = Aw\left(A^{(1)}A^{(3)}l^f\Big/\sqrt{2}+A^{(2)}A^{(3)}l^f+\sqrt{2}A^{(1)}A^{(2)}l^{f(3)}\right)\Big/A^b \tag{A.6}$$

$$c_7 = AA^{(1)}A^{(2)}w\left(1-1/\sqrt{2}\right)l^f\Big/A^b \tag{A.7}$$

$$c_8 = AA^{(3)}l^{f^2} \tag{A.8}$$

$$c_9 = A\left(A^{(1)}A^{(2)}l^f l^{f(3)}\Big/\sqrt{2}+A^{(2)}A^{(3)}wl^f+\sqrt{2}A^{(1)}A^{(2)}wl^{f(3)}\right)\Big/A^b \tag{A.9}$$

$$c_{10} = A\left(-A^{(1)}A^{(3)}l^f l^{f(3)}\Big/\sqrt{2}+A^{(1)}A^{(3)}wl^f\right)\Big/A^b \tag{A.10}$$

$$c_{11} = A\left(A^{(1)}1A^{(2)}l^f l^{f(3)}\Big/\sqrt{2}+A^{(1)}A^{(3)}wl^f+\sqrt{2}A^{(1)}A^{(2)}wl^{f(3)}\right)\Big/A^b \tag{A.11}$$

$$c_{12} = A\left(-A^{(2)}A^{(3)}l^f l^{f(3)}\Big/\sqrt{2}+A^{(2)}A^{(3)}wl^f\right)\Big/A^b \tag{A.12}$$

$$c_{13} = \sqrt{2}lA^{(3)}A^b \tag{A.13}$$

$$c_{14} = AA^b l^{f(3)} \tag{A.14}$$

$$c_{15} = AA^{(3)}w \tag{A.15}$$

References

Baum, G.A., Brennan, D.C., Habeger, C.C., 1981. Orthotropic elastic constants of paper. Tappi J. 64 (8).
Beex, L.A.A., Peerlings, R.H.J., Geers, M.G.D., 2011. A quasicontinuum methodology for multiscale analyses of discrete microstructural models. Int. J. Numer. Methods Eng. 87, 701–718.
Bergander, A., Salmèn, L., 2002. Cell wall properties and their effects on the mechanical properties of fibers. J. Mater. Sci. 37, 151–156.
Bronkhorst, C.A., 2003. Modelling paper as a two-dimensional elastic–plastic stochastic network. Int. J. Solids Struct. 40, 5441–5454.
Cox, H., 1952. The elasticity and strength of paper and other fibrous materials. Br. J. Appl. Phys. 3, 72.
Hashin, Z., 1983. Analysis of composite materials – a survey. J. Appl. Mech. 50, 481–505.

Kulachenko, A., Uesaka, T., 2012. Direct simulations of fiber network deformation and failure. Mech. Mater. 51, 1–14.
Larsson, P.A., Wagberg, L., 2008. Influence of fibre–fibre joint properties on the dimensional stability of paper. Cellulose 15, 515–525.
Liu, J., Chen, Z., Li, K., 2010. A 2-D lattice model for simulating the failure of paper. Theor. Appl. Fract. Mech. 54, 1–10.
Liu, J.X., Chen, Z.T., Wang, H., Li, K.C., 2011. Elasto-plastic analysis of influences of bond deformability on the mechanical behavior of fiber networks. Theor. Appl. Fract. Mech. 55, 131–139.
Nanri, Y., Uesaka, T., 1993. Dimensional stability of mechanical pulps – drying shrinkage and hygroexpansivity. Tappi J. 76, 62–66.
Niskanen, K., 1998. Paper Physics. Fapet Oy Helsinki, Finland.
Niskanen, K., 2011. Mechanics of Paper Products. Walter de Gruyter Incorporated.
Ostoja-Starzewski, M., 1998. Random field models of heterogeneous materials. Int. J. Solids Struct. 35, 2429–2455.
Ostoja-Starzewski, M., Stahl, D., 2000. Random fiber networks and special elastic orthotropy of paper. J. Elast. Phys. Sci. Solids 60, 131–149.
Ramasubramanian, M.K., Wang, Y., 2007. A computational micromechanics constitutive model for the unloading behavior of paper. Int. J. Solids Struct. 44, 7615–7632.
Rosen, B.W., Hashin, Z., 1970. Effective thermal expansion coefficients and specific heats of composite materials. Int. J. Eng. Sci. 8, 157–173.
Roylance, D., 1996. Mechanics of Materials. Wiley and Sons.
Schulgasser, K., Page, D.H., 1988. The influence of transverse fibre properties on the in-plane elastic behaviour of paper. Compos. Sci. Technol. 32, 279–292.
Stahl, D.C., Cramer, S.M., 1998. A three-dimensional network model for a low density fibrous composite. J. Eng. Mater. Technol. 120, 126–130.
Strömbro, J., Gudmundson, P., 2008. Mechano-sorptive creep under compressive loading a micromechanical model. Int. J. Solids Struct. 45, 2420–2450.
Strömbro, J., Gudmundson, P., 2008. An anisotropic fibre-network model for mechano-sorptive creep in paper. Int. J. Solids Struct. 45, 5765–5787.
Uesaka, T., 1994. General formula for hygroexpansion of paper. J. Mater. Sci. 29, 2373–2377.
Uesaka, T., Qi, D., 1994. Hygroexpansivity of paper – effects of fibre to fibre bonding. J. Pulp Paper Sci. 20, J175–J179.
Viguiè, J., Dumont, P.J.J., Mauret, E., Rolland du Roscoat, S., Vacher, P., Desloges, I., Bloch, J.-F., 2011. Analysis of the hygroexpansion of a lignocellulosic fibrous material by digital correlation of images obtained by X-ray synchrotron microtomography: application to a folding box board. J. Mater. Sci. 46, 4756–4769.
Wilbrink, D.V., Beex, L.A.A., Peerlings, R.H.J., 2013. A discrete network model for bond failure and frictional sliding in fibrous materials. Int. J. Solids Struct. 50, 1354–1363.